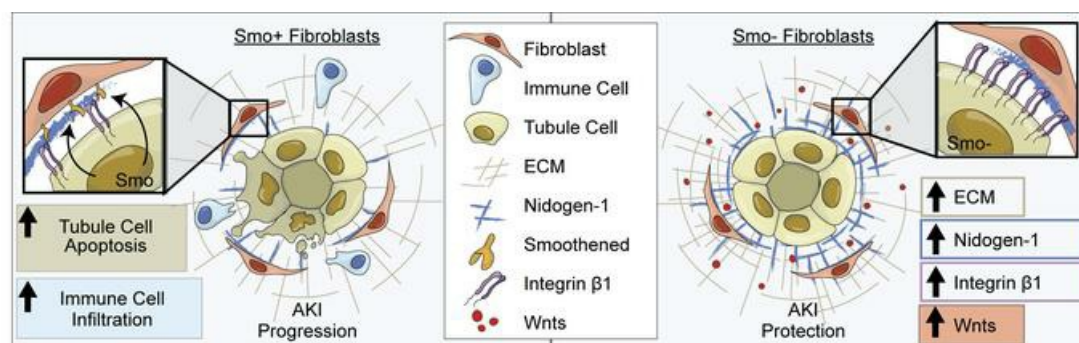# Fibroblast expression of transmembrane protein smoothened governs microenvironment characteristics after acute kidney injury

Yuan Gui, … , Youhua Liu, Dong Zhou

Research In-Press Preview **Nephrology**

Graphical abstract

Fibroblast expression of transmembrane protein smoothened governs microenvironment characteristics after acute kidney injury

Yuan Gui[1], Haiyan Fu[2], Zachary Palanza[1], Jianling Tao[3], Yi-Han Lin[4], Wenjian Min[5], Yi Qiao[6], Christopher Bonin[7], Geneva Hargis[7], Yuanyuan Wang[1], Peng Yang[5], Donald L. Kreutzer[6], Yanlin Wang[1], Yansheng Liu,[8,9] Yanbao Yu[10], Youhua Liu[2], Dong Zhou[1]

1. Division of Nephrology, Department of Medicine, University of Connecticut School of Medicine, Farmington, CT, 06030, USA;
2. Department of Pathology, University of Pittsburgh School of Medicine, Pittsburgh, PA, 15261, USA;
3. Division of Nephrology, Department of Medicine, Stanford University School of Medicine, Stanford, CA, 94305, USA;
4. National Center for Advancing Translational Sciences, Rockville, MD, 20850, USA;
5. State Key Laboratory of Natural Medicines and Jiangsu Key Laboratory of Drug Design and Optimization, China Pharmaceutical University, Nanjing, China;
6. Department of Surgery, University of Connecticut School of Medicine, Farmington, CT, 06030, USA;
7. University of Connecticut, School of Medicine, Farmington, CT, 06030, USA;
8. Yale Cancer Biology Institute, Yale University, West Haven, Connecticut, USA;
9. Department of Pharmacology, School of Medicine, Yale University, New Haven, Connecticut, USA;
10. Department of Chemistry & Biochemistry, University of Delaware, Newark, DE, 19716, USA.

Drs. Haiyan Fu and Youhua Liu's Present Address: State Key Laboratory of Organ Failure Research, National Clinical Research Center of Kidney Disease, Division of Nephrology, Nanfang Hospital, Southern Medical University, Guangzhou, 510515, China.

The authors have declared that no conflict of interest exists.

Running Title: Loss of fibroblast-derived smoothened protects against AKI.

Abstract: 149

Word count: 5,235

To whom correspondence should be addressed:
Dong Zhou, M.D., Ph.D., Division of Nephrology, Department of Medicine, University of Connecticut School of Medicine, 263 Farmington Ave, L1062, Farmington, CT, 06030, Phone: 860-679-3254, Email: dzhou@uchc.edu; or Youhua Liu, Ph.D., Department of Pathology, University of Pittsburgh School of Medicine, 200 Lothrop St, BST-S405, Pittsburgh, PA, 15261, Email: liuyh@smu.edu.cn; or Yanbao Yu, Ph.D. Department of Chemistry & Biochemistry, University of Delaware, Newark, DE, 19716, Phone: 302-831-2465, Email: yybyu@udel.edu.

Abstract:

The smoothened (Smo) receptor facilitates hedgehog signaling between kidney fibroblasts and tubules during acute kidney injury (AKI). Tubule-derived hedgehog is protective in AKI, but the role of fibroblast-selective Smo is unclear. Here, we report that Smo-specific ablation in fibroblasts reduced tubular cell apoptosis and inflammation, enhanced perivascular mesenchymal cells activities, and preserved kidney function after AKI. Global proteomics of these kidneys identified extracellular matrix proteins, and nidogen-1 glycoprotein in particular, as key response markers to AKI. Intriguingly, Smo was bound to nidogen-1 in cells, suggesting that loss of Smo could impact nidogen-1 accessibility. Phosphoproteomics revealed that the 'AKI protector' Wnt signaling pathway was activated in these kidneys. Mechanistically, nidogen-1 interacted with integrin β1 to induce Wnts in tubules to mitigate AKI. Altogether, our results support that fibroblast-selective Smo dictates AKI fate through cell-matrix interactions, including nidogen-1, and offers a robust resource and path to further dissect AKI pathogenesis.

Introduction:

Acute kidney injury (AKI) is a clinical syndrome characterized by an abrupt decline in renal function within a few hours or days, which is associated with high morbidity and mortality globally (1). Although developing effective treatments for human AKI remains a challenge, advances in research have widened our knowledge of the pathogenesis of this refractory disease. In AKI induced by ischemia, sepsis, nephrotoxins, or major surgery, renal tubules have been the well-acknowledged epicenter of damage (2). However, emerging evidence shows that resident perivascular mesenchymal cells, such as fibroblasts and pericytes, are instinctively mobilized to participate in the repair process once AKI occurs (3-6). Unfortunately, the role of fibroblasts in AKI remains a mystery.

Fibroblasts are becoming increasingly appreciated for their association with AKI prognosis (7-9). Studies have demonstrated that after AKI, fibroblast activation precedes tubular cell proliferation (4). Early activated fibroblasts immediately release signals to neighboring cells, such as tubular epithelial or other perivascular mesenchymal cells, to rescue kidneys from AKI through auto- or paracrine mechanisms. Several highly conserved cell signaling systems are recruited for the acute phase of kidney injury/repair, including Hedgehog (Hh), Wnt, Notch, and mammalian target of rapamycin (3, 10-16). Moreover, fibroblasts are the principal effector cells responsible for synthesizing the extracellular matrix (ECM) (17). After AKI, appropriate types and amounts of ECM are beneficial for forming a favorable microenvironment in the diseased kidneys (18). This microenvironment functionally serves as a physical home to allow injured cells to rest and as a scaffold backbone for tissue remodeling. Therefore, it is conceivable to speculate that fibroblasts have a unique role in regulating AKI recovery.

3

Smoothened (Smo) is a seven-pass transmembrane receptor that is a crucial positive regulator in the Hh signaling pathway. The Hh pathway is a highly evolutionarily conserved system linked to cell-cell communications for embryonic development and adult tissue homeostasis (19, 20). Its activity is triggered by stoichiometric binding of Hh ligands to Patched (Ptc) (21). Ptc itself is an inhibitory transmembrane receptor that keeps the Hh pathway off by inhibiting Smo in the absence of Hh (22). Once Hh is presented to Ptc, Smo is activated which turns on downstream genes such as the glioma-associated oncogene homolog (Gli) transcription factor. Mammals have three Hh homologues, Desert (Dhh), Indian (Ihh), and Sonic (Shh), of which Shh is the best studied (23, 24). In the kidney, Shh is exclusively produced by tubules (4, 25), but fibroblasts are its specific target (26). In these responsive fibroblasts, how Smo regulates AKI remains unclear. Besides transducing signals, we ask whether fibroblast-selective Smo directly impacts kidney protection by binding small molecules or large proteins to adjust cell behaviors and even the tissue microenvironment after AKI. Here, integrating traditional molecular pathology with systems biology, we illustrate how fibroblast-selective Smo controls kidney fate after AKI. From the perspective of cell-matrix-cell interactions, our study provides open-access data resources as a complementary piece of the puzzle for understanding AKI pathogenesis.

Results

***Smo* ablation in fibroblasts mitigates ischemic AKI**

To elucidate the role of fibroblast-selective *Smo* in AKI, we generated two strains of fibroblast-specific *Smo* knockout mice by employing the tamoxifen-inducible Cre-LoxP system (11). Briefly, as depicted in Figure 1A, homozygous *Smo*-floxed mice were mated with the *Gli1*-CreER[T2] or platelet-

4

derived growth factor receptor β (*Pdgfrβ*)-P2A-CreER[T2] transgenic mice under the control of endogenous *Gli1* or *Pdgfrβ* promoter to create *Smo* fibroblast conditional knockout mice (genotype: Cre^{+/-}, *Smo*^{fl/fl}; designated as *Gli1-Smo-/-* or *Pdgfrβ-Smo-/-*); *Gli1* or *Pdgfrβ* expression is confined to a subset of fibroblasts (Figure 1A) (3, 11, 27-29). Age and sex-matched *Smo*-floxed mice (genotype: Cre^{-/-}, *Smo*^{fl/fl}; designated as *Gli1-Smo+/+* or *Pdgfrβ-Smo+/+*) from the same litters were used as controls (Supplementary Figure S1A–S1B). *Gli1-Smo-/-* and *Pdgfrβ-Smo-/-* mice were phenotypically normal. After tamoxifen injections for five consecutive days, Cre-mediated recombination was induced in *Gli1+* or *Pdgfrβ+* fibroblasts, as previously reported (11, 30-32). To confirm the knockout efficiency, we further isolated primary kidney fibroblasts from the above mice (~10 days old) and deleted *Smo* using hydroxytamoxifen. Quantitative real-time PCR (qPCR) and western blot analyses demonstrated marked reductions of Smo in the isolated fibroblasts from *Gli1-Smo-/-* and *Pdgfrβ-Smo- /-* mice (Figure 1B). There was no appreciable abnormality and difference in body weight, kidney-to-body weight ratios, serum creatinine, and blood pressures between *Gli1-Smo+/+* and *Gli1-Smo-/-* or *Pdgfrβ-Smo+/+* and *Pdgfrβ-Smo-/-* mice (Figure 1C and 1D). Then, after 1-week tamoxifen wash-out, the mice were subjected to 30 minutes of bilateral renal ischemia-reperfusion injury (IRI) to induce AKI and allowed to recover for 1 day. Surprisingly, in contrast with deletion of Shh in tubules (4), deletion of *Smo* in Gli1+ fibroblasts preserved kidney function at 1 day after ischemic AKI. Compared to *Gli1-Smo+/+* mice subjected to ischemic AKI, serum creatinine levels were reduced by 22.7% in *Gli1-Smo-/-* mice following ischemic AKI (Figure 1E). Consistently, *Gli1-Smo-/-* mice exhibited reduced AKI-associated morphologic changes, such as less cellular debris, brush border loss, and intratubular proteinaceous casts (Figure 1F; Quantitative data shown in Supplementary Figure S2A). Furthermore, the expression of the classic acute tubular injury marker, neutrophil gelatinase-associated

5

lipocalin (NGAL) (33), was also decreased in *Gli1-Smo-/-* mice at 1 day after ischemic AKI, compared to *Gli1-Smo+/+* mice (Figure 1G; Quantitative data shown in Supplementary Figure S2B).

To confirm the above phenotypic changes, we assessed the differences in the key biological mechanisms involved in AKI development — inflammation and cell death (34, 35) — between *Gli1-Smo+/+* and *Gli1-Smo-/-* mice ischemic kidneys. qPCR analysis revealed that tumor necrosis factor-α (*Tnfα*), monocyte chemoattractant protein-1 (*Mcp1*), and regulated on activation, normal T cell expressed and secreted (*Rantes*) mRNA levels were markedly reduced in *Gli1-Smo-/-* mice, compared with *Gli1-Smo+/+* mice (Figure 1H). Accordingly, immunostaining results indicated fewer infiltrated CD45^{+} monocytes and CD3^{+} T cells in *Gli1-Smo-/-* mice diseased kidneys (Figure 1F; Quantitative data in Supplementary Figure S2C and S2D).

Because AKI features sublethal or lethal damage of kidney tubules (35), we further examined if loss of *Smo* in *Gli1+* fibroblasts influence different types of tubular cell death in ischemic kidneys, such as apoptosis, necrosis, or ferroptosis. Western blots revealed that pro-apoptosis proteins FasL and Bad were reduced in *Gli1-Smo-/-* mice, compared with *Gli1-Smo+/+* mice (Figure 1G; Quantitative data shown in Supplementary Figure S2B). Terminal deoxynucleotidyl transferase dUTP nick end labeling (TUNEL) showed similar results (Figure 1F; Quantitative data in Supplementary Figure S2E). Intriguingly, neither Glutathione Peroxidase 4 (GPX4) nor phosphorylated mixed lineage kinase domain-like protein (pMLKL) was changed between *Gli1-Smo+/+* and *Gli1-Smo-/-* kidneys after ischemic AKI (Supplementary Figure S2F–S2G).

Similar to the findings in *Gli1-Smo-/-* mice, after IRI at 1 day, *Pdgfrβ-Smo-/-* mice also exhibited preserved serum creatinine levels (31.4% reduction, Figure 1I), reduced protein expression of NGAL, FasL, and Bad (Figure 1J), and improved secretion of chemocytokines (Figure 1K) compared with

Pdgfrβ-Smo+/+ mice. PAS staining, TUNEL assay, and immunohistochemical staining against CD45 consistently confirmed the results (Figure 1L). The quantitative data is presented in Supplementary Figure S2H–S2K. Collectively, these results suggested that ablation of *Smo* in *Gli1+* or *Pdgfrβ+* fibroblasts protect against ischemic AKI.

Loss of *Smo* in fibroblasts enhance perivascular mesenchymal cell activity after AKI

Hh/Smo/Gli1 signaling is necessary for fibroblast proliferation in various diseases such as kidney/ liver/lung/heart fibrosis, systemic sclerosis, and cancer microenvironment formation (25, 36-42). We previously reported that early activated fibroblasts are indispensable for kidney repair after AKI (4). Therefore, we were puzzled as to why loss of fibroblast-selective *Smo* alleviated AKI in our current model. Considering *Gli1+* or *Pdgfrβ+* fibroblasts are a small fraction of the perivascular mesenchymal cell population (11, 30), we speculated that loss of Smo in *Gli1+* or *Pdgfrβ+* fibroblasts may naturally activate the remaining perivascular mesenchymal cells as compensation, such as non-*Gli1+* and non-*Pdgfrβ+* fibroblasts/pericytes, to enhance cell survival after AKI. To this end, we systemically assessed the expression of several markers for activated fibroblasts/pericytes in diseased kidneys, including fibroblast-specific protein 1 (Fsp1), vimentin, α-smooth muscle actin (αSma), and Pdgfrβ. qPCR analyses revealed that mRNA expression of *Fsp1*, *vimentin*, and *αSma* were substantially increased in *Gli1-Smo-/-* mice 1 day after IRI, compared with *Gli1-Smo+/+* mice (Figure 2A). Consistently, *Pdgfrβ-Smo-/-* mice showed similar results after IRI (Figure 2B). Western blots further demonstrated marked elevation of Pdgfrβ, vimentin, or α-SMA proteins in *Gli1-Smo-/-* or *Pdgfrβ-Smo-/-* mice (Figure 2C–2D; quantitative data are presented in Supplementary Figure S3A and S3C). Consistently, immunostaining revealed increased expression of Pdgfrβ or vimentin in *Gli1-Smo-/-* or *Pdgfrβ-Smo-/-*

mice diseased kidneys (Figure 2E–2F; quantitative data are presented in Supplementary Figure S3B and S3D). To understand the distribution of proliferative cells in diseased kidneys after loss of Smo in *Gli1+* or *Pdgfrβ+* fibroblasts, we assessed proliferating cell nuclear antigen (PCNA) and Ki67 levels. Western blot assays demonstrated an upregulation of PCNA in *Gli1-Smo-/-* or *Pdgfrβ-Smo-/-* mice at 1 day after IRI compared with their corresponding littermate controls (Figure 2C–2D; quantitative data are presented in Supplementary Figure S3A and S3C), and immunohistochemical staining further confirmed that the number of Ki67+ or PCNA+ interstitial cells were larger in *Gli1-Smo-/-* or *Pdgfrβ-Smo-/-* kidneys (Figure 2E–2F). Taken together, these results indicated that ablation of *Smo* in fibroblasts in turn activated perivascular mesenchymal cells after ischemic AKI.

Global proteomics identifies nidogen-1 as a key participant in AKI repair after loss of *Smo* in fibroblasts

To better understand how loss of *Smo* in fibroblasts mitigates AKI, we used a label-free quantitative approach to profile the global proteome of *Gli1-Smo+/+* and *Gli1-Smo-/-* mice kidneys at 1 day after IRI (Figure 3A). Impressively, the principal component analysis (PCA) of our proteomic data clearly classified *Gli1-Smo+/+* and *Gli1-Smo-/-* mice according to their genotype (Figure 3B; quantified proteins are presented in Supplementary Table S1). A 2-tailed t-test identified 660 differentially expressed proteins (Permutation FDR 0.05) between *Gli1-Smo+/+* and *Gli1-Smo-/-* mice diseased kidneys. Compared to *Gli1-Smo+/+* mice, 241 and 419 proteins were up- and down-regulated, respectively, in *Gli1-Smo-/-* mice (Figure 3C and Supplementary Table S2; Correlations between biological replicates within the same group and the distribution of protein intensity are presented in Supplementary Figure S4A–S4B). The following Gene Ontology (GO) cellular compartment analysis

8

revealed that these proteins were generally distributed in mitochondrion, extracellular exosome, peroxisome, cytosol, and ECM (Figure 3D). The activation of perivascular mesenchymal cells in *Gli1-Smo-/-* mice is linked to enhanced ECM synthesis in diseased kidneys (Figure 2). Indeed, unlike most proteins that showed down-regulated trends in other cellular compartments, 110 out of 141 ECM proteins were upregulated in *Gli1-Smo-/-* mice compared with *Gli1-Smo+/+* mice (Figure 3D). This phenomenon indicates that ECM remodeling by enhanced protein synthesis may play a critical role in *Gli1-Smo-/-* kidney repair after IRI.

We therefore focused on the activated ECM proteins with significant up-regulations in *Gli1-Smo-/-* mice kidneys. To select the most significantly impacted ECM protein for further investigation, we excluded those that have been well studied [such as vimentin (Figure 2) and prelamin-A/C]. Among the remaining proteins, we paid our attention to nidogen-1 (NID1), one of the most prominent matrix proteins upregulated in *Gli1-Smo-/-* mice (Figure 3E–3F and Supplementary Figure S4C) which has been reported as an essential component of the basement membrane that plays a role in cell interactions with the ECM. Since ECM is identified as a major cellular compartment of distributed proteins, we hypothesized that ECM could organize a favorable kidney local microenvironment to repair kidneys after AKI. Thus, we chose NID1 for further study.

To confirm our findings, we assessed NID1 levels in *Gli1-Smo+/+* and *Gli1-Smo-/-* or *Pdgfrβ-Smo+/+* and *Pdgfrβ-Smo-/-* mice. After IRI at 1 day, NID1 protein was induced in diseased kidneys compared with sham controls. Western blot assays demonstrated a marked elevation of NID1 protein in *Gli1-Smo-/-* or *Pdgfrβ-Smo-/-* mice (Figure 3G–3H; quantitative data are presented in Supplementary Figure S4D and S4E), compared with their corresponding controls. In a separate analysis using single nucleus RNA sequencing, NID1 was highly expressed in fibroblasts/pericytes

9

after IRI at 12 hours (Figure 3I) (43). Consistently, immunohistochemical staining confirmed enhanced NID1 distribution in the interstitium of *Gli1-Smo-/-* or *Pdgfrβ-Smo-/-* ischemic kidneys (Figure 3J). To further establish the molecular link between NID1 and Smo, we identified multiple potential binding sites of NID1 and Smo in the optimal conformation at pose 51 through virtual protein-protein ZDOCK and RDOCK algorithms (Supplementary Figure S5). Immunoprecipitation of Smo or NID1 pulled down NID1 or Smo, respectively, which indicated Smo physically binds to NID1 (Figure 3K). In addition, to obtain a broader view of the dysregulated pathways after loss of Smo in fibroblasts, we constructed a signaling network based on the STRING database. The analysis with the highest confidence score (cutoff = 0.9) resulted in 413 nodes and 1815 interactions. (Supplementary Figure 4F). The majority of interactions and nodes were associated with Wnt, Hh, and fatty acid oxidation pathways. Collectively, these data suggested that loss of Smo in fibroblasts results in upregulation of NID1, which may orchestrate a favorable matrix and metabolic microenvironment to mitigate AKI.

Phosphoproteomics reveals that Smo deletion in fibroblasts remodels the Wnt signaling pathway

To gain more insights into the temporal regulation and functional changes in signaling of *Smo-*deficient fibroblasts in AKI repair, we performed phosphoproteomics on the same set of kidney samples used for the global proteomics (Figure 4A). Similar to the global proteomics, PCA of the phosphoproteome clearly separated *Gli1-Smo+/+* and *Gli1-Smo-/-* mice kidneys (Figure 4B). Impressively, most of the significantly different phosphopeptides were decreased in *Gli1-Smo-/-* mice compared with *Gli1-Smo+/+* mice (Supplementary Table S3). We then filtered the phosphorylation data set to include those phosphopeptides that were quantified in at least three replicates and used t-test analysis with p-value correction (Permutation FDR 0.05). Enrichment analysis indicated that

phosphoproteins associated with RNA splicing, cell-cell adhesion, and mRNA processing were significantly over-represented ($p < 10^{-5}$). Consistent with network analysis performed with global proteomics (Supplementary Figure S4F), a clear reduced phosphorylating of multiple components of the Wnt signaling pathway in *Gli1-Smo-/-* mice was observed (Supplementary Figure S6A). Pairwise comparisons between *Gli1-Smo+/+* and *Gli1-Smo-/-* mice at 1 day after IRI highlighted substantially changed components in the Wnt signaling pathway, such as pGSK3β, pSlc9a3r1, pCtnnd1, pTGFβ1i1, pCcny, and pLeo1 (Figure 4C and Supplementary Figure S6B–S6C). In particular, we identified two downregulated tyrosine phosphorylation sites (Tyr216 and Tyr279) on GSK-3β in *Gli1-Smo-/-* mice. Dephosphorylation on Tyr216 and Tyr279 represses the activity of GSK-3β. Therefore, in *Gli1-Smo-/-* mice, inactivated GSK-3β loses its capacity to destabilize β-catenin, a principal protein in the Wnt signaling pathway. This ultimately causes the activation of the canonical Wnt/β-catenin signaling pathway. In addition, the network analysis showed that GSK-3β interacts with other proteins in *Gli1-Smo-/-* kidneys as well (Supplementary Figure S6B).

Previously, we and others reported that activation of the Wnt signaling pathway protected against AKI (10, 12, 14, 44). Based on the information provided by the phosphoproteome analysis, we assessed the status of the canonical Wnt signaling pathway in *Gli1-Smo+/+* and *Gli1-Smo-/-* mice after AKI. qPCR revealed that 9 out of 19 Wnt family members (*Wnt 2, 4, 5A, 5B, 7A, 7B, 9B, 10A,* and *11*) were markedly induced in *Gli1-Smo-/-* mice (Figure 4D). In the same kidneys, several Frizzled receptors in the Wnt signaling pathway were also upregulated in *Gli1-Smo-/-* mice (Supplementary Figure S7A). Western blots demonstrated that β-catenin, Wnt 1, or Wnt 5A/B proteins were markedly induced in *Gli1-Smo-/-* as well as *Pdgfrβ-Smo-/-* mice kidneys after IRI (Figure 4E and 4F; quantitative data are presented in Supplementary Figure S7B and S7C). Immunohistochemical staining further

confirmed increased expression of β-catenin, Wnt1, Wnt4, or Wnt5A/B in *Gli1-Smo-/-* and *Pdgfrβ-Smo-/-* mice kidney tubular cells, compared with their corresponding littermate controls (Figure 4G). Of particular interest, we saw impressive inductions of Wnt1, Wnt4, Wnt5A/B in the biopsy specimens from AKI patients (Figure 4H). Taken together, our data suggest that ablation of Smo in fibroblasts is linked to Wnt signaling pathway activation after ischemic AKI.

Integrin β1 may link nidogen 1 and the Wnt signaling pathway after AKI

Given specifically deleting Smo in fibroblasts induced interstitial matrix protein NID1 and simultaneously activated the Wnt signaling pathway in tubules after AKI, we sought to explore the possible connection between NID1 and Wnts. As a prominent matrix glycoprotein with potential roles in tissue regeneration (45), NID1 often plays a role in cell interactions with the extracellular matrix by activating specific receptors, such as integrins, while integrin receptors could synergize with the Wnt signaling pathway to form a loop to control tissue injury/repair and tumor metastasis (46, 47). So, we systemically evaluated the expression of 6 integrin receptors linked to tubular cells (48, 49), including integrin α3, α6, αV, α8, β1, and β6, in *Gli1-Smo+/+* and *Gli1-Smo-/-* mice after ischemic AKI. Impressively, only integrin β1 was induced in the diseased kidneys between *Gli1-Smo+/+* and *Gli1-Smo-/-* mice (Figure 5A). Of note, at baseline, integrin β1 was barely detectable in the sham controls. After IRI, compared with *Gli1-Smo+/+* or *Pdgfrβ-Smo+/+* mice, integrin β1 was markedly induced in *Gli1-Smo-/-* or *Pdgfrβ-Smo-/-* mice kidneys (Figure 5B–5E). Immunohistochemical staining consistently showed upregulated integrin β1 in *Gli1-Smo-/-* and *Pdgfrβ-Smo-/-* mice kidney tubular cells, compared with their corresponding littermate controls (Figure 5F). Meanwhile, both NID1 and integrin β1 were increased in the biopsy specimens from AKI patients (Figure 5G).

To validate our findings in ischemic AKI, we constructed a separate AKI mouse model induced by cisplatin (Figure 6A). At 3 days after cisplatin injection, compared to the corresponding controls, serum creatinine levels were reduced by 38.7% or 36.8% in *Gli1-Smo-/-* or *Pdgfrβ-Smo-/-* mice, respectively (Figure 6B–6C). Western blot analysis, TUNEL assay, and histological/immunostaining demonstrated improved kidney morphological changes and reduce cell apoptosis and inflammatory cell infiltration in *Gli1-Smo-/-* or *Pdgfrβ-Smo-/-* mice (Figure 6D–6G; quantitative data in Supplementary Figure S8A–S8D). Consistent with IRI model, NID1, Wnt1, and integrin β1 were also increased in *Gli1-Smo-/-* or *Pdgfrβ-Smo-/-* mice kidneys after cisplatin injection, compared to *Gli1-Smo+/+* or *Pdgfrβ-Smo+/+* mice (Figure 6H–6L). These results indicated that tubular-derived integrin β1 is a potential mechanistic clue in elucidating the connection between NID1 and Wnts after various insults caused-AKI.

Genetic knockdown or pharmaceutical inhibition of Smo in fibroblasts promotes tubular cell survival through NID1 in vitro and ex vivo

To further decipher the role of fibroblast-selective Smo in regulating tubular cell survival, normal rat kidney fibroblasts (NRK-49F) were transfected with Dicer-substrate Smo siRNA (Supplementary Figure S9A) or treated with cyclopamine (CPN), a small-molecule inhibitor of Smo. Under hypoxia stress induced by $CoCl_2$, knocking down or blocking Smo activity promoted the expression of PDGFR-β, vimentin, α-SMA, and PCNA proteins in the cultured fibroblasts (Figure 7A and 7B). Meanwhile, NID1 protein was induced in the same set of cell lysates (Figure 7C and 7D), and immunofluorescence staining of whole cells showed similar results (Figure 7E and Supplementary Figure S9B). Quantitatively, enzyme-linked immunosorbent assay revealed that NID1 concentration was higher in

the conditioned medium (CM) collected from the cultured fibroblasts after incubation with CPN under hypoxic stresses, compared to vehicles (Figure 7F).

To validate our in vivo findings that loss of fibroblast-selective Smo induced tubular Wnts and promoted cell survival, we performed several in vitro and ex vivo experiments. In vitro, we first treated normal rat kidney epithelial cells (NRK-52E) with NID1-enriched CM collected from Smo-knockdown or CPN-treated fibroblasts (Figure 7G). Under basal conditions, NID1-enriched CM did not cause dramatic changes in the expression of β-catenin, Wnt1, Wnt2, and Wnt5A/B in NRK-52E cells (Supplementary Figure S9C and S9D). However, these proteins were markedly induced under hypoxic stress after incubated with NID1-enriched CM (Figure 7H and 7I). Second, we applied NID1 recombinant protein to treat NRK-52E at different dosages, as depicted in Figure 7G. NID1 activated β-catenin, Wnt1, Wnt5A/B, and Wnt16 in both basal and hypoxic conditions (Figure 7J and 7K). Impressively, either NID1-enriched CM or NID1 recombinant protein possessed the capacity to reduce tubular cell apoptosis. Specifically, less caspase 3 cleavage was detected in NRK-52E cells after treatment with NID1-enriched CM or NID1 recombinant protein after being stimulated with a classic apoptosis inducer, staurosporine (Figure 7L, 7M, and 7O). Immunofluorescence staining for cleaved caspase-3 confirmed these findings (Figure 7N, 7P, and Supplementary Figure S9F; quantitative data in Figure 7Q and Supplementary Figure S9E and S9G).

To better mimic the in vivo microenvironment, we decellularized cultured fibroblasts (Control, Smo-knockdown, or CPN-treated) after hypoxia stress for 24 hours to obtain matrix scaffolds. Then, seeding NRK-52E cells onto the scaffold-coated plate (Figure 8A), as we did in previous studies (50). NID1 was markedly enriched in the decellularized matrix scaffold isolated from Smo-knockdown or CPN-treated fibroblasts (Figure 8B). Under basal conditions, there were minor differences in β-catenin,

14

Wnt 2, and Wnt 5A/B expression in the seeded tubular cells between control scaffolds and NID1-enriched scaffolds (Supplementary Figure S10A and S10B). Under hypoxic stress, the NID1-enriched scaffold exhibited an enhanced capacity to activate β-catenin, Wnt 2, and Wnt 5A/B and repress caspase-3 cleavage in NRK-52E cells (Figure 8C–8F). Mechanistically, NID1-enriched CM/matrix scaffold or NID1 recombinant protein activated integrin β1 in the tubular cells (Figure 8G–8I), whereas knockdown of integrin β1 repressed β-catenin accumulation which resulted in inactivation of the canonical Wnt signaling pathway and consequently increased cleaved-caspase 3 levels in tubular cells (Figure 8J–8K and Supplementary Figure S10C). To confirm the above findings, we further performed a molecular docking study. A strong binding site with extremely low dock energy between NID1 and integrin β1 was identified, the site formed a dense hydrogen bonding network system to stabilize the bindings (Figure 8L and Supplementary Figure S11A-S11B). Then, we mutated 5 amino acids in NID1 protein sequences that mainly contributed to the binding and substituted them with A (Figure 8M and Supplementary Figure S11C). Detailed information is presented in the Supplemental Methods. We then treated NRK-52E cells with mutant or active NID1, and we observed that mutant NID1 failed to induce β-catenin compared to the active NID1 under hypoxic stresses, because it could not bind integrin β1 receptor (Figure 8N). Similar to the result using integrin β1 knockdown approach, mutant NID1 increased cleaved-caspase 3 levels in tubular cells after staurosporine stimulation (Figure 8O). Taken together, our results suggest that inhibiting Smo in fibroblasts liberated NID1 to activate the Wnt signaling pathway in tubules through integrin β1. This, in turn, created a favorable kidney local microenvironment to prevent or mitigate AKI (Figure 8P).

Discussion

15

Although the kidney is a vulnerable organ that has limited regenerative capacity, there is consensus that the tubular epithelium can repair damage to the kidney after AKI (2, 51). The mechanisms involved are rigorously debated. For a long time, proximal tubule progenitors were thought to exist in various locations such as bone marrow, the renal interstitium, and the renal papilla (2). In recent years, the concept of kidney perivascular mesenchymal cells contributing to tubule repair in AKI has been increasingly appreciated (3, 4, 7, 11), although many unknowns remain. In this study, combining conditional knockout mice, in vitro and ex vivo models, and systems biology approaches, we illustrated that fibroblasts play an important role in protecting against AKI. Our results indicate that ablation of *Smo* in *Gli1*+ or *Pdgfrβ*+ fibroblasts 1) mitigates AKI caused by IRI or cisplatin, 2) promotes perivascular mesenchymal cells activation, 3) upregulates NID1 and activates the Wnt signaling pathway in tubules, and 4) reveals that integrin β1 may bridge NID1 and the Wnt signaling pathway in tubules, which may explain reduced tubular cell death and increased cell survival after AKI.

Smo is one of the multi-span transmembrane proteins in the core reception system for the Hh pathway (52, 53). It has been well documented that Hh controls cell growth and differentiation through a highly conserved signal transduction pathway which reciprocally travels between producing and responsive cells (20, 27, 54). In the kidney, deleting Shh in producing tubular cells aggravates AKI (4), whereas the current study surprisingly shows that loss of Smo in Hh-responding fibroblasts mitigates tubular cell apoptosis and inflammatory cell infiltration after AKI (Figure 1 and 6). These opposing observations reflect the challenge of elucidating AKI if focused on a single signaling pathway or cell type. What we observed was of particular interest: after AKI, loss of Smo in fibroblasts activated substantial perivascular mesenchymal cells such as non-*Gli1*+/*Pdgfrβ*+ fibroblasts, pericytes, and mesenchymal stromal cells (Figure 2). The number of proliferative interstitial cells in Smo

16

conditional knockout mice is apparently more than their corresponding littermate controls, indicating interstitial cells' potential in mitigating AKI. But why did the loss of Smo in fibroblasts in turn activate perivascular mesenchymal cells after AKI? There are two possibilities. One is that because our conditional knockout mouse models were generated by an inducible Cre-LoxP system in which *Gli1+* or *Pdgfrβ+* fibroblasts are a small fraction of the entire population of perivascular mesenchymal cells (11, 32, 55). Therefore, after AKI, these non-*Gli1+* or non-*Pdgfrβ+* fibroblast subpopulations are instinctively mobilized to rescue themselves and their neighboring cells, such as tubular cells. Second, these early and overactivated fibroblasts can immediately synthesize matrix proteins and initiate a favorable kidney local microenvironment (KLM) through multiple mechanisms such as cell mechanical changes (56), and by simultaneously recruiting growth factors from other cell types such as tubule-derived Wnts and Hh (Figure 3 and 4). These growth factors may further fibroblast activities by a transient feedback loop. However, defining the subpopulation of fibroblast is a really challenging job due to the highly heterogeneous nature of cells. The current study still lacks analysis at the single-cell level to fully fill the gap in elucidating the phenomena of fibroblast overactivation in *Gli1-Smo-/-* and *Pdgfrβ-Smo-/-* mice kidneys after AKI.

AKI is a refractory clinical syndrome. Therefore, its repair process is certainly to involve multi-cellular/non-cellular components. Consistent with the enhanced activation of perivascular mesenchymal cells in *Gli1-Smo-/-* or *Pdgfrβ-Smo-/-* kidneys (Figure 2), global proteomics confirmed that ECM is a key cellular compartment where differentially expressed proteins are distributed after ischemic AKI (Figure 3). As a three-dimensional non-cellular component in the kidney, ECM provides the biophysical scaffolding for the kidney and biochemical or mechanical microenvironment to control cell homeostasis and differentiation (57-59). The number of markedly upregulated ECM proteins in

Gli1-Smo-/- mice is nearly 3.5-fold more than in their littermate controls (Figure 3). These quantitative analyses suggest perivascular mesenchymal cells synthesized an appropriate amount of ECM to reconstruct kidneys under acute ischemic stress. Among these identified ECM markers, NID1 is one of the most prominent matrix proteins increased in *Gli1-Smo-/-* and *Pdgfrβ-Smo-/-* mice (Figure 3). NID1, formerly known as entactin, is an essential structural component of the basement membrane and ECM. The basement membrane is a specialized layer of ECM components in the kidney that plays a central role in maintaining organ functions (60). Our data showed that NID1 is predominantly localized in kidney interstitium after AKI (Figure 3). Thus far, most studies have focused on secretion of NID1 preventing cancer metastasis. Sporadic studies have reported that NID1 mitigates ischemia and promotes heart survival and regeneration after injury (45, 61). Consistent with the positive roles NID1 plays in treating various diseases, our data provides additional evidence for a role of NID1 in AKI and kidney repair as well.

Another interesting finding of our study is that Smo physically binds NID1 to form a protein-protein complex. As a frizzled-class G-protein-coupled receptor (GPCR), Smo contains two distinct ligand-binding sites: one in its heptahelical transmembrane domain (TMD) and another one in the extracellular cysteine-rich domain (62). The TMD binding site is known to bind the small-molecule Smo-specific inhibitor, CPN (63). In comparison, whether a GPCR could physically link to macromolecules like NID1, integrate into the basement membrane, and subsequently give them unique functions in diseased kidneys is unclear. We showed through immunoprecipitation that Smo binds to NID1 (Figure 3). Therefore, in the absence of Smo, NID1 protein would be released (Figure 7), and then deposited in the neighboring epithelial basement membranes. Basement membranes are essential ECM structures shaped by the networks of collagen type IV and laminins, both of which are linked by

18

NID1 (45). This strategic subcellular localization of NID1 enables it to mediate cell attachment and communications between cells and ECM (64-66). We also demonstrated in our in vitro and ex vivo systems that increased NID1 reduced tubular cell apoptosis and promoted cell survival (Figure 7 and 8).

Considering the visual pathological effects of AKI repair, it is undeniable that the fibroblast-ECM-tubule interaction is a standard process of building a favorable KLM, which is complex, heterotypic, and dynamic (67). We need to ask whether NID1-enriched KLM plays a role in repairing AKI. In this study, we utilized a decellularized scaffold that retains fibroblast's overall architecture to closely imitate the in vivo matrix microenvironment. NID1-enriched scaffold activated the Wnt signaling pathway and reduced tubular cell death (Figure 8). Most importantly, these biological capacities of NID1 in protecting against AKI were accomplished by strongly binding to tubular integrin β1 receptor, thereby forming a loop with Wnts signals in tubules (Figure 5, 6, and 8). Our global and phosphoproteomics data coincidentally provided us with solid information that the Wnt signaling pathway was dramatically activated in *Gli1-Smo-/-* mice after AKI. As we know, at the early phase of AKI, most Wnt family proteins are activated in tubules and exhibit a protective role in preserving kidney function (12). Of note, the canonical Wnt signaling is controlled by protein phosphorylation and dephosphorylation. Here, we identified the downregulated tyrosine phosphorylation sites (Tyr216 and Tyr279) on GSK-3β, destabilizing β-catenin in *Gli1-Smo-/-* mice after AKI (Figure 4). Phosphorylation-dependent β-catenin degradation is a key step in turning off the Wnt signaling pathway (68, 69). Besides GSK-3β, the extent of phosphorylation of Dishevelled protein and low-density lipoprotein receptor-related proteins, the activities of the Axin–scaffold phospho-destruction complex, and the modulation of kinases such as nemo-like kinase and homeodomain-

19

interacting protein serine/threonine kinases can impact gene-specific β-catenin recruitment and its transcription (70). In addition, our phosphoproteomics identified cell-cell adhesion as a markedly changed biological event in *Gli1-Smo-/-* mice after AKI. This cell-cell adhesion is worth further investigation, given the connection between NID1 and integrin β1 demonstrated in the current system.

Our study has some limitations. First, the core reception system for Hh signaling includes two multispan transmembrane proteins—Ptc and Smo—and Hh reciprocally controls them. Ptc inhibits Smo in the absence of Hh. In the presence of Hh, Hh binds Ptc to release its inhibition of Smo, leading to Smo phosphorylation and activation. However, whether loss of fibroblast-selective Smo influences Ptc in AKI repair was not studied here. Second, we observed increased fatty acid oxidation in *Gli1-Smo-/-* mice after AKI, but how disrupting Smo affects energy metabolism after AKI remains unclear. Third, the *Gli1* or *Pdgfrβ* promoter in the Cre-LoxP system limited the population of the target fibroblasts. So, we cautiously described the *Gli1+* or *Pdgfrβ+* fibroblasts in relatively broad terms by encompassing perivascular mesenchymal cells, pericytes, and fibroblasts. More robust genetic animal models and omics analyses at the single-cell level are needed to define these cell populations in AKI. Lastly, while this study posits that *Gli1+* or *Pdgfrβ+* fibroblast-Smo deletion results in activation of non-*Smo-/-* fibroblasts, upregulation of NID1, and activation of the Wnt signaling pathway in tubule epithelial cells, we did not mechanistically test how non-*Smo-/-* fibroblasts were activated. Still, our results provide some mechanistic insight into the link between Smo, NID1, Wnt signaling, and AKI mitigation, and offer additional pathways that we will pursue in future experiments.

In summary, using a multidisciplinary approach, we report that loss of Smo in *Gli1+* or *Pdgfrβ+* fibroblasts protect against AKI through ECM-cell interactions involving multiple signaling pathways. We highlight the importance of creating a favorable tissue microenvironment in determining AKI

prognosis. Our findings provide preclinical stage strategies to understand AKI better and shed light on effectively restoring kidney functions.

Methods

The detailed information of methodology, usage of chemical and biological reagents, antibodies, and nucleotide sequences of the primers is presented in the Supplementary Methods.

Sex as a biological variable

Our AKI study exclusively examined male mice because female mice represented greater resistance than male mice against renal ischemia-reperfusion injury and cisplatin-induced toxicity. Human kidney biopsy samples were obtained from both male and female subjects. It is unknown whether the findings in male mice are relevant to female mice.

Statistics

All data were expressed as mean $\pm$ SEM if not specified otherwise in the legends. Statistical analysis of the data was performed using GraphPad Prism 9 (GraphPad Software, San Diego, CA). Comparison between two groups was made using a two-tailed Student's t-test or the Rank Sum Test if data failed a normality test. Statistical significance for multiple groups was assessed by one-way ANOVA, followed by the Student-Newman-Keuls test. Results are presented in dot plots, with dots denoting individual values. $P < 0.05$ was considered statistically significant.

Study approval

All animal experiments were performed in accordance with institutional and federal guidelines and approved by the Institutional Animal Care Committee of the University of Pittsburgh, School of Medicine (Protocol number: 16048123) and the University of Connecticut, School of Medicine (Protocol number: AP-200105-0923).

Data availability

Data are available in the Supporting Data Values XLS file. Raw Mass Spectrometry data were deposited in MassIVE with the data set identifier MSV000088609. (doi:10.25345/C5NS23).

Authors Contributions

YG and DZ conceived the project. YG and DZ wrote and revised the manuscript. YG, HF, ZP, JT, YQ, and YW performed most of the in vivo, ex vivo, in vitro studies involving mRNA expression analysis, Western blotting assay, immunostaining and imaging. YL, YY, and YL performed proteomic analysis. WM and PY performed docking study. YG, CB, GH, DK, YW, YL, and DZ edited the manuscript. DZ supervised the entire project.

Acknowledgments

the manuscript.

Disclosure

The authors declare no conflict of interest.

References

1. Ronco C, Bellomo R, and Kellum JA. Acute kidney injury. *Lancet.* 2019;394(10212):1949-64.

2. Little M, and Humphreys B. Regrow or Repair: An Update on Potential Regenerative Therapies for the Kidney. *J Am Soc Nephrol.* 2021.

3. Kramann R, Wongboonsin J, Chang-Panesso M, Machado FG, and Humphreys BD. Gli1(+) Pericyte Loss Induces Capillary Rarefaction and Proximal Tubular Injury. *J Am Soc Nephrol.* 2017;28(3):776-84.

4. Zhou D, Fu H, Liu S, Zhang L, Xiao L, Bastacky SI, et al. Early activation of fibroblasts is required for kidney repair and regeneration after injury. *FASEB J.* 2019;33(11):12576-87.

5. Chou YH, Pan SY, Shao YH, Shih HM, Wei SY, Lai CF, et al. Methylation in pericytes after acute injury promotes chronic kidney disease. *J Clin Invest.* 2020;130(9):4845-57.

6. Schiessl IM, Grill A, Fremter K, Steppan D, Hellmuth MK, and Castrop H. Renal Interstitial Platelet-Derived Growth Factor Receptor-beta Cells Support Proximal Tubular Regeneration. *J Am Soc Nephrol.* 2018;29(5):1383-96.

7. Humphreys BD, and Bonventre JV. Mesenchymal stem cells in acute kidney injury. *Annu Rev Med.* 2008;59:311-25.

8. Boor P, and Floege J. The renal (myo-)fibroblast: a heterogeneous group of cells. *Nephrol Dial Transplant.* 2012;27(8):3027-36.

9. Humphreys BD. Kidney injury, stem cells and regeneration. *Curr Opin Nephrol Hypertens.* 2014;23(1):25-31.

10. Lin SL, Li B, Rao S, Yeo EJ, Hudson TE, Nowlin BT, et al. Macrophage Wnt7b is critical for kidney repair and regeneration. *Proc Natl Acad Sci U S A.* 2010;107(9):4194-9.

11. Zhou D, Fu H, Xiao L, Mo H, Zhuo H, Tian X, et al. Fibroblast-Specific beta-Catenin Signaling Dictates the Outcome of AKI. *J Am Soc Nephrol.* 2018;29(4):1257-71.

12. Zhou D, Li Y, Lin L, Zhou L, Igarashi P, and Liu Y. Tubule-specific ablation of endogenous beta-catenin aggravates acute kidney injury in mice. *Kidney Int.* 2012;82(5):537-47.

13. Gui Y, Lu Q, Gu M, Wang M, Liang Y, Zhu X, et al. Fibroblast mTOR/PPARgamma/HGF axis protects against tubular cell death and acute kidney injury. *Cell Death Differ.* 2019;26(12):2774-89.

14. Schunk SJ, Floege J, Fliser D, and Speer T. WNT-beta-catenin signalling - a versatile player in kidney injury and repair. *Nat Rev Nephrol.* 2021;17(3):172-84.

15. Sirin Y, and Susztak K. Notch in the kidney: development and disease. *J Pathol.* 2012;226(2):394-403.

16. Wyss JC, Kumar R, Mikulic J, Schneider M, Aebi JD, Juillerat-Jeanneret L, et al. Targeted gamma-secretase inhibition of Notch signaling activation in acute renal injury. *Am J Physiol Renal Physiol.* 2018;314(5):F736-F46.

17. Frangogiannis NG. Fibroblast-Extracellular Matrix Interactions in Tissue Fibrosis. *Curr Pathobiol Rep.* 2016;4(1):11-8.

18. Chen S, Fu H, Wu S, Zhu W, Liao J, Hong X, et al. Tenascin-C protects against acute kidney injury by recruiting Wnt ligands. *Kidney Int.* 2019;95(1):62-74.

19. Chung SI, Moon H, Ju HL, Cho KJ, Kim DY, Han KH, et al. Hepatic expression of Sonic Hedgehog induces liver fibrosis and promotes hepatocarcinogenesis in a transgenic mouse model. *J Hepatol.* 2016;64(3):618-27.

20. Zhou D, Tan RJ, and Liu Y. Sonic hedgehog signaling in kidney fibrosis: a master communicator. *Sci China Life Sci.* 2016;59(9):920-9.

21. Marigo V, Davey RA, Zuo Y, Cunningham JM, and Tabin CJ. Biochemical evidence that patched is the Hedgehog receptor. *Nature.* 1996;384(6605):176-9.

22. Gong X, Qian H, Cao P, Zhao X, Zhou Q, Lei J, et al. Structural basis for the recognition of Sonic Hedgehog by human Patched1. *Science.* 2018;361(6402).

23. Lum L, and Beachy PA. The Hedgehog response network: sensors, switches, and routers. *Science.* 2004;304(5678):1755-9.

24. Guerrero I, and Ruiz i Altaba A. Development. Longing for ligand: hedgehog, patched, and cell death. *Science.* 2003;301(5634):774-6.

25. Zhou D, Li Y, Zhou L, Tan RJ, Xiao L, Liang M, et al. Sonic hedgehog is a novel tubule-derived growth factor for interstitial fibroblasts after kidney injury. *J Am Soc Nephrol.* 2014;25(10):2187-200.

26. Ding H, Zhou D, Hao S, Zhou L, He W, Nie J, et al. Sonic hedgehog signaling mediates epithelial-mesenchymal communication and promotes renal fibrosis. *J Am Soc Nephrol.* 2012;23(5):801-13.

27. Fabian SL, Penchev RR, St-Jacques B, Rao AN, Sipila P, West KA, et al. Hedgehog-Gli pathway activation during kidney fibrosis. *Am J Pathol.* 2012;180(4):1441-53.

28. Steele NG, Biffi G, Kemp SB, Zhang Y, Drouillard D, Syu L, et al. Inhibition of Hedgehog Signaling Alters Fibroblast Composition in Pancreatic Cancer. *Clin Cancer Res.* 2021;27(7):2023-37.

29. Tsukui T, Ueha S, Shichino S, Hashimoto S, Nakajima T, Shiraishi K, et al. Gli signaling pathway modulates fibroblast activation and facilitates scar formation in pulmonary fibrosis. *Biochem Biophys Res Commun.* 2019;514(3):684-90.

30. Kramann R, Schneider RK, DiRocco DP, Machado F, Fleig S, Bondzie PA, et al. Perivascular Gli1+ progenitors are key contributors to injury-induced organ fibrosis. *Cell Stem Cell.* 2015;16(1):51-66.

31. Zhou D, Fu H, Zhang L, Zhang K, Min Y, Xiao L, et al. Tubule-Derived Wnts Are Required for Fibroblast Activation and Kidney Fibrosis. *J Am Soc Nephrol.* 2017;28(8):2322-36.

32. Kuppe C, Ibrahim MM, Kranz J, Zhang X, Ziegler S, Perales-Paton J, et al. Decoding myofibroblast origins in human kidney fibrosis. *Nature.* 2021;589(7841):281-6.

33. Soni SS, Cruz D, Bobek I, Chionh CY, Nalesso F, Lentini P, et al. NGAL: a biomarker of acute kidney injury and other systemic conditions. *Int Urol Nephrol.* 2010;42(1):141-50.

34. Rabb H, Griffin MD, McKay DB, Swaminathan S, Pickkers P, Rosner MH, et al. Inflammation in AKI: Current Understanding, Key Questions, and Knowledge Gaps. *J Am Soc Nephrol.* 2016;27(2):371-9.

35. Linkermann A, Chen G, Dong G, Kunzendorf U, Krautwald S, and Dong Z. Regulated cell death in AKI. *J Am Soc Nephrol.* 2014;25(12):2689-701.

36. Horn A, Palumbo K, Cordazzo C, Dees C, Akhmetshina A, Tomcik M, et al. Hedgehog signaling controls fibroblast activation and tissue fibrosis in systemic sclerosis. *Arthritis Rheum.* 2012;64(8):2724-33.

37. Bolanos AL, Milla CM, Lira JC, Ramirez R, Checa M, Barrera L, et al. Role of Sonic Hedgehog in idiopathic pulmonary fibrosis. *Am J Physiol Lung Cell Mol Physiol.* 2012;303(11):L978-90.

38. Hanna A, and Shevde LA. Hedgehog signaling: modulation of cancer properies and tumor mircroenvironment. *Mol Cancer.* 2016;15:24.

39.   Jung Y, McCall SJ, Li YX, and Diehl AM. Bile ductules and stromal cells express hedgehog ligands and/or hedgehog target genes in primary biliary cirrhosis. *Hepatology.* 2007;45(5):1091-6.

40.   Machado MV, and Diehl AM. Hedgehog signalling in liver pathophysiology. *J Hepatol.* 2018;68(3):550-62.

41.   O'Sullivan ED, Mylonas KJ, Xin C, Baird DP, Carvalho C, Docherty MH, et al. Indian Hedgehog release from TNF-activated renal epithelia drives local and remote organ fibrosis. *Sci Transl Med.* 2023;15(698):eabn0736.

42.   Gu D, Soepriatna AH, Zhang W, Li J, Zhao J, Zhang X, et al. Activation of the Hedgehog signaling pathway leads to fibrosis in aortic valves. *Cell Biosci.* 2023;13(1):43.

43.   Kirita Y, Wu H, Uchimura K, Wilson PC, and Humphreys BD. Cell profiling of mouse acute kidney injury reveals conserved cellular responses to injury. *Proc Natl Acad Sci U S A.* 2020;117(27):15874-83.

44.   Kawakami T, Ren S, and Duffield JS. Wnt signalling in kidney diseases: dual roles in renal injury and repair. *J Pathol.* 2013;229(2):221-31.

45.   Zbinden A, Layland SL, Urbanczyk M, Carvajal Berrio DA, Marzi J, Zauner M, et al. Nidogen-1 Mitigates Ischemia and Promotes Tissue Survival and Regeneration. *Adv Sci (Weinh).* 2021;8(4):2002500.

46.   Tejeda-Munoz N, Morselli M, Moriyama Y, Sheladiya P, Pellegrini M, and De Robertis EM. Canonical Wnt signaling induces focal adhesion and Integrin beta-1 endocytosis. *iScience.* 2022;25(4):104123.

47.   Giacomelli C, Jung J, Wachter A, Ibing S, Will R, Uhlmann S, et al. Coordinated regulation of WNT/beta-catenin, c-Met, and integrin signalling pathways by miR-193b controls triple negative breast cancer metastatic traits. *BMC Cancer.* 2021;21(1):1296.

48.   Pozzi A, and Zent R. Integrins in kidney disease. *J Am Soc Nephrol.* 2013;24(7):1034-9.

49.   Kreidberg JA, and Symons JM. Integrins in kidney development, function, and disease. *Am J Physiol Renal Physiol.* 2000;279(2):F233-42.

50.   Fu H, Tian Y, Zhou L, Zhou D, Tan RJ, Stolz DB, et al. Tenascin-C Is a Major Component of the Fibrogenic Niche in Kidney Fibrosis. *J Am Soc Nephrol.* 2017;28(3):785-801.

51.   Little MH. Regrow or repair: potential regenerative therapies for the kidney. *J Am Soc Nephrol.* 2006;17(9):2390-401.

52. Chen Y, and Jiang J. Decoding the phosphorylation code in Hedgehog signal transduction. *Cell Res.* 2013;23(2):186-200.

53. Li S, Li S, Wang B, and Jiang J. Hedgehog reciprocally controls trafficking of Smo and Ptc through the Smurf family of E3 ubiquitin ligases. *Sci Signal.* 2018;11(516).

54. Kramann R, Fleig SV, Schneider RK, Fabian SL, DiRocco DP, Maarouf O, et al. Pharmacological GLI2 inhibition prevents myofibroblast cell-cycle progression and reduces kidney fibrosis. *J Clin Invest.* 2015;125(8):2935-51.

55. E Oh, Wu H, Muto Y, Donnelly EL, Machado FG, Fan LX, et al. A conditionally immortalized Gli1-positive kidney mesenchymal cell line models myofibroblast transition. *Am J Physiol Renal Physiol.* 2019;316(1):F63-F75.

56. Gui Y, Palanza Z, Gupta PR, Li H, Pan Y, Wang Y, et al. Calponin 2 regulates ketogenesis to mitigate acute kidney injury. *JCI Insight.* 2023.

57. Frantz C, Stewart KM, and Weaver VM. The extracellular matrix at a glance. *J Cell Sci.* 2010;123(Pt 24):4195-200.

58. Marastoni S, Ligresti G, Lorenzon E, Colombatti A, and Mongiat M. Extracellular matrix: a matter of life and death. *Connect Tissue Res.* 2008;49(3):203-6.

59. Bulow RD, and Boor P. Extracellular Matrix in Kidney Fibrosis: More Than Just a Scaffold. *J Histochem Cytochem.* 2019;67(9):643-61.

60. Jandl K, Mutgan AC, Eller K, Schaefer L, and Kwapiszewska G. The basement membrane in the cross-roads between the lung and kidney. *Matrix Biol.* 2021.

61. Willem M, Miosge N, Halfter W, Smyth N, Jannetti I, Burghart E, et al. Specific ablation of the nidogen-binding site in the laminin gamma1 chain interferes with kidney and lung development. *Development.* 2002;129(11):2711-22.

62. Byrne EFX, Sircar R, Miller PS, Hedger G, Luchetti G, Nachtergaele S, et al. Structural basis of Smoothened regulation by its extracellular domains. *Nature.* 2016;535(7613):517-22.

63. Taipale J, Chen JK, Cooper MK, Wang B, Mann RK, Milenkovic L, et al. Effects of oncogenic mutations in Smoothened and Patched can be reversed by cyclopamine. *Nature.* 2000;406(6799):1005-9.

64. Yurchenco PD, and Patton BL. Developmental and pathogenic mechanisms of basement membrane assembly. *Curr Pharm Des.* 2009;15(12):1277-94.

65. Yi XY, Wayner EA, Kim Y, and Fish AJ. Adhesion of cultured human kidney mesangial cells to native entactin: role of integrin receptors. *Cell Adhes Commun.* 1998;5(3):237-48.

66. Mao X, Tey SK, Yeung CLS, Kwong EML, Fung YME, Chung CYS, et al. Nidogen 1-Enriched Extracellular Vesicles Facilitate Extrahepatic Metastasis of Liver Cancer by Activating Pulmonary Fibroblasts to Secrete Tumor Necrosis Factor Receptor 1. *Adv Sci (Weinh).* 2020;7(21):2002157.

67. Fu H, Gui Y, Liu S, Wang Y, Bastacky SI, Qiao Y, et al. The hepatocyte growth factor/c-met pathway is a key determinant of the fibrotic kidney local microenvironment. *iScience.* 2021;24(10):103112.

68. Liu C, Li Y, Semenov M, Han C, Baeg GH, Tan Y, et al. Control of beta-catenin phosphorylation/degradation by a dual-kinase mechanism. *Cell.* 2002;108(6):837-47.

69. Khan S, Kwak YT, Peng L, Hu S, Cantarel BL, Lewis CM, et al. NLRP12 downregulates the Wnt/beta-catenin pathway via interaction with STK38 to suppress colorectal cancer. *J Clin Invest.* 2023;133(19).

70. Verheyen EM, and Gottardi CJ. Regulation of Wnt/beta-catenin signaling by protein kinases. *Dev Dyn.* 2010;239(1):34-44.
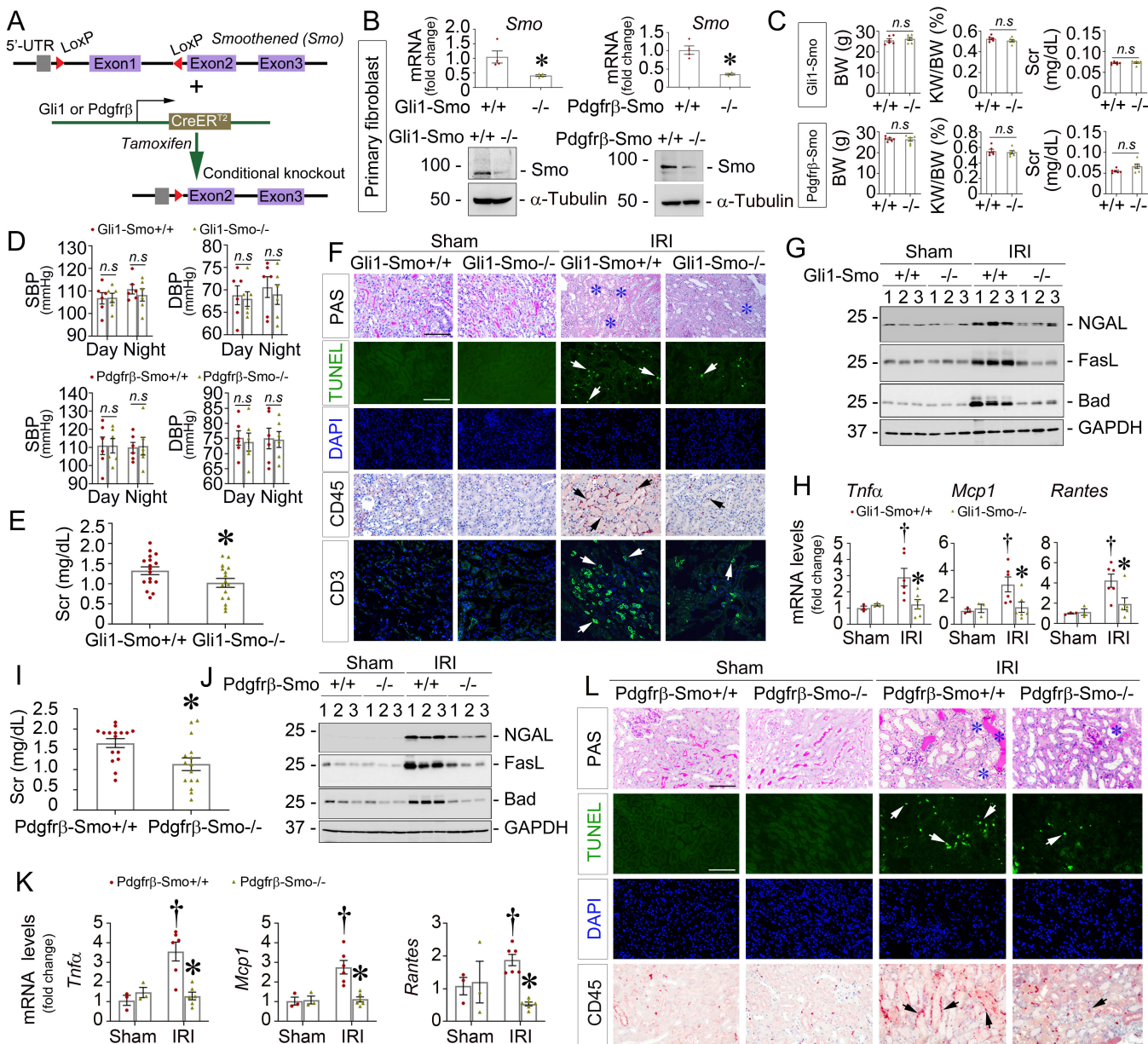
Figure 1: Fibroblast-specific ablation of Smo mitigates ischemic AKI. (A) Generation of Smo fibroblast-specific deletion mice. (B) Quantitative real-time PCR (qPCR) analysis (n = 4) and western blot assay showing Smo levels in primary fibroblasts isolated from Gli1-Smo+/+ and Gli1-Smo-/- or Pdgfrβ-Smo+/+ and Pdgfrβ-Smo-/- kidneys. (C) The mouse baseline body weight (BW), kidney-to-body weight (KW/BW) ratios, serum creatinine (Scr), and (D) blood pressure levels (n = 6). At 1 day after IRI, (E) Scr levels in Gli1-Smo+/+ and Gli1-Smo-/- mice (n=16-17). (F) Periodic Acid–Schiff (PAS) staining showing kidney morphological changes in Gli1-Smo+/+ and Gli1-Smo-/- mice. Blue asterisks indicate injured tubules. Representative micrographs of TUNEL or immunohistochemical staining against CD45 and CD3 in Gli1-Smo+/+ and Gli1-Smo-/- kidneys. (G) Western blots assay of NGAL, FasL, and Bad in Gli1-Smo+/+ and Gli1-Smo-/- kidneys (Sham, n = 3; IRI, n = 5). (H) qPCR analysis showing Tnfα, Mcp1, and Rantes mRNA levels in Gli1-Smo+/+ and Gli1-Smo-/- kidneys (Sham, n = 3; IRI, n = 5). (I) Scr levels in Pdgfrβ-Smo+/+ and Pdgfrβ-Smo-/- mice (n = 15-16). (J) Western blots showing NGAL, FasL, and Bad levels in Pdgfrβ-Smo+/+ and Pdgfrβ-Smo-/- kidneys. (K) qPCR analysis showing Tnfα, Mcp1, and Rantes mRNA levels in Pdgfrβ-Smo+/+ and Pdgfrβ-Smo-/- kidneys (Sham, n = 3; IRI, n = 6). (L) Representative micrographs of PAS, TUNEL, and immunohistochemical staining against CD45 in Pdgfrβ-Smo+/+ and Pdgfrβ-Smo-/- kidneys. Scale bar, 25 µm. Arrows indicate positive cells. DAPI is a nuclear counterstain. For all western blot panels, numbers indicate individual animals in a given group. † P < 0.05 versus sham control, * P < 0.05 versus Gli1-Smo+/+ or Pdgfrβ-Smo+/+ IRI mice. Dots indicate individual animals in a given group. Graphs are presented as means ± SEM. Differences among groups were analyzed using unpaired t-tests or one-way ANOVA followed by the Student-Newman-Keuls test.
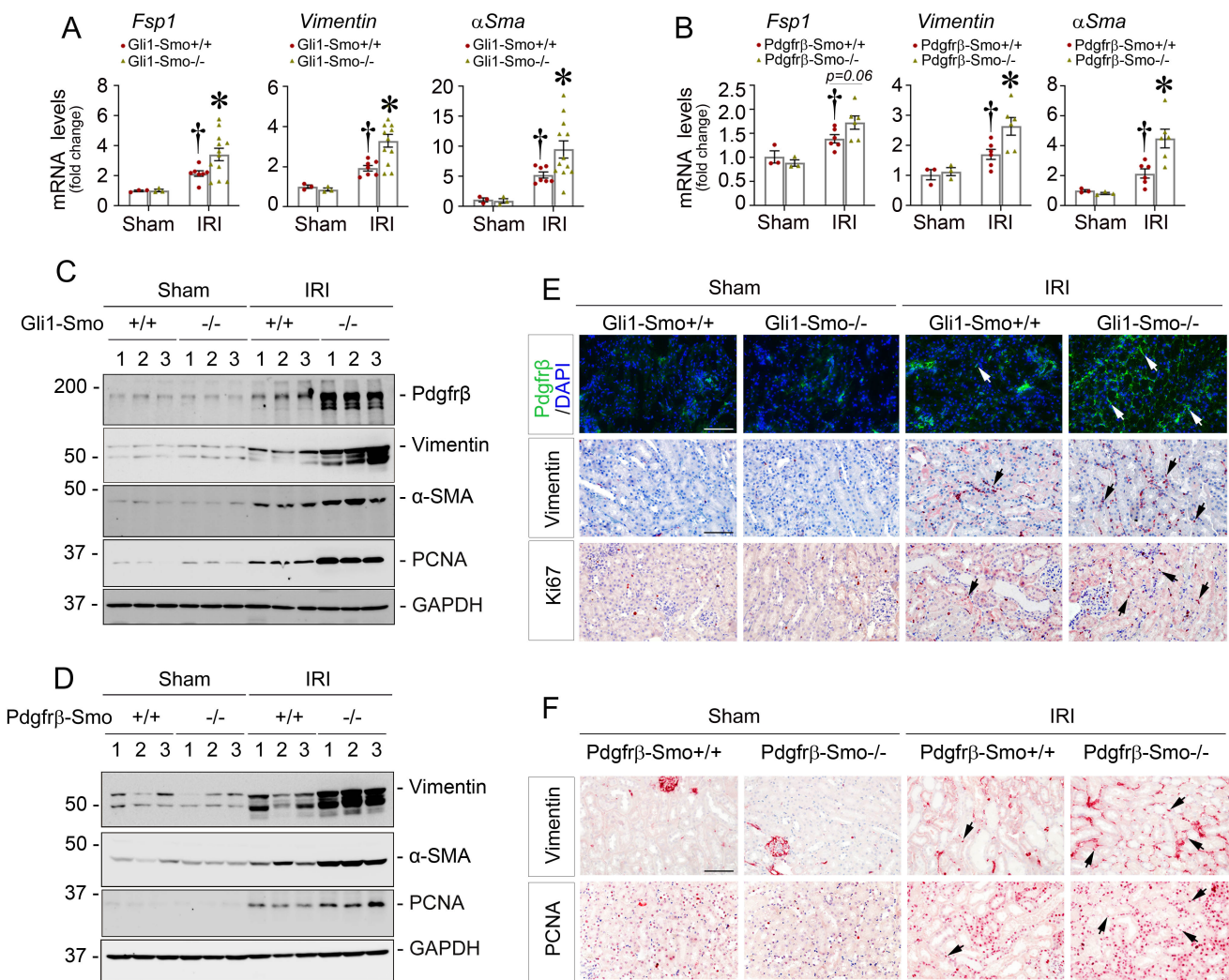
Figure 2: Fibroblast-specific ablation of Smo promotes perivascular mesenchymal cell activation and proliferation after AKI. At 1 day after IRI, (A) qPCR analyses of Fsp1, vimentin, and αSma mRNA in Gli1-Smo+/+ and Gli1-Smo-/- kidneys (Sham, n = 3; IRI, n = 7-12). (B) qPCR analyses of Fsp1, vimentin, and αSma mRNA in Pdgfrβ-Smo+/+ and Pdgfrβ-Smo-/- kidneys (Sham, n = 3; IRI, n = 6). (C) Western blots assay of Pdgfrβ, vimentin, αSMA, and PCNA proteins in Gli1-Smo+/+ and Gli1-Smo-/- kidneys. (D) Western blots assay of vimentin, α-SMA, and PCNA proteins in Pdgfrβ-Smo+/+ and Pdgfrβ-Smo-/- kidneys. (E) Representative micrographs of Pdgfrβ, vimentin, and Ki67 expression in Gli1-Smo+/+ and Gli1-Smo-/- kidneys. Arrows indicate positive cells. (F) Representative micrographs of vimentin and PCNA expression in Pdgfrβ-Smo+/+ and Pdgfrβ-Smo-/- kidneys. Scale bar, 25 µm. Arrows indicate positive cells. DAPI is a nuclear counterstain. For all western blot panels, numbers indicate individual animals in a given group. † P < 0.05 versus sham control, * P < 0.05 versus Gli1-Smo+/+ or Pdgfrβ-Smo+/+ IRI mice. Dots indicate individual animals in a given group. Graphs are presented as means ± SEM. Differences among groups were analyzed using one-way ANOVA, followed by the Student-Newman-Keuls test.
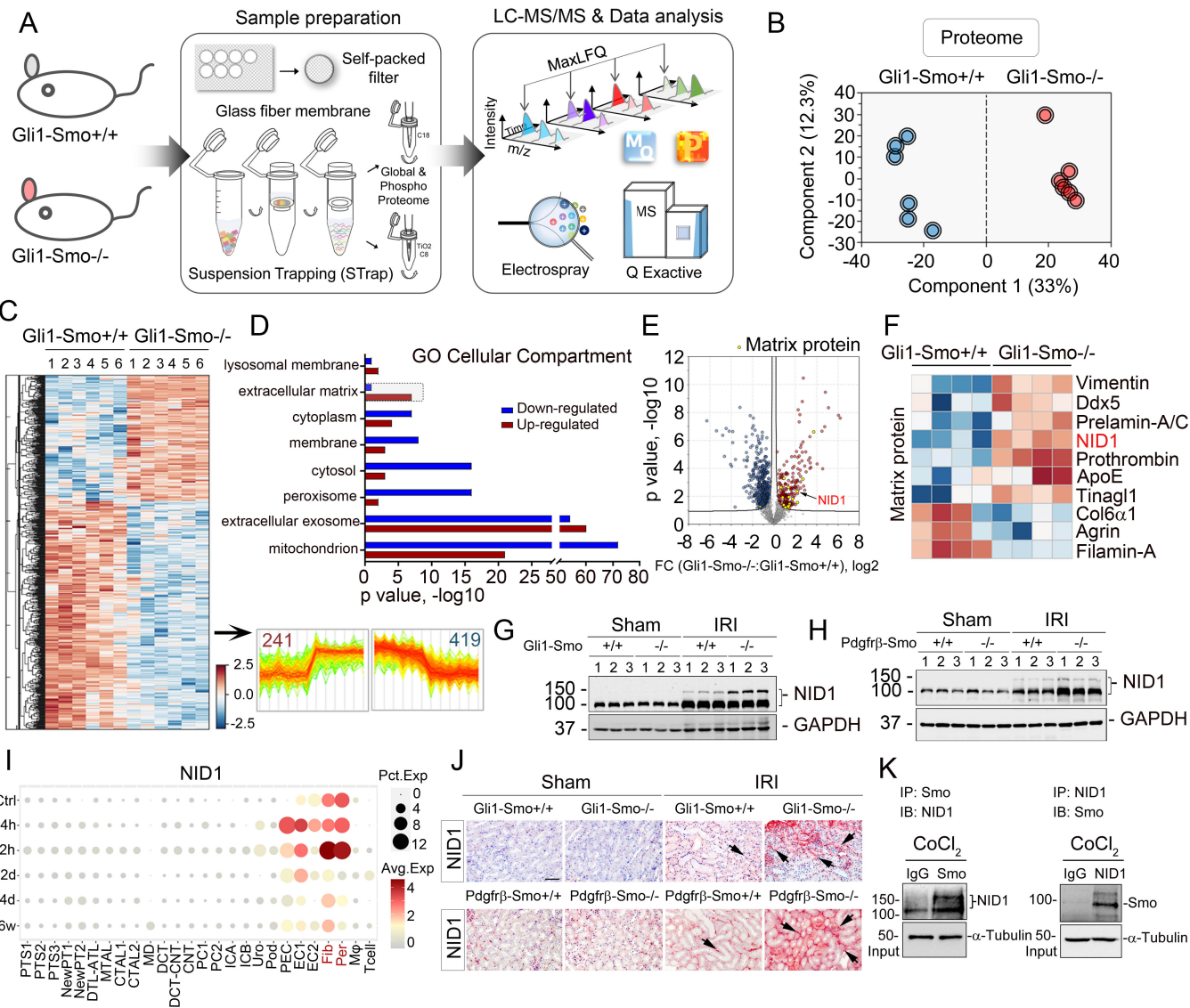
Figure 3: Global proteomics identifies Nidogen-1 (NID1) as a prominent matrix protein in Gli1+ fibroblast-specific Smo deletion kidneys after AKI. (A) Experimental workflow of the global proteomic analysis. Six mice in each group were used for mass spectrometry. (B) Principal component analysis of global proteomes from Gli1-Smo+/+ and Gli1-Smo-/- kidneys 1 day after ischemic AKI. (C) Heatmap of ANOVA significant proteins. Label-free quantitation (LFQ) intensity of represented proteins were z-scored and plotted according to the color bar. Two clusters of proteins with different patterns of abundance profiles are highlighted in the heatmap. (D) Gene Ontology (GO) cellular compartment terms in each cluster of proteins are plotted with their names and significance. ECM proteins are boxed to indicate the protein group with the largest difference in upregulated proteins. (E) Volcano plot shows the differential proteins between Gli1-Smo+/+ and Gli1-Smo-/- kidneys. Up- and down-regulated proteins (fold-change, FC) are colored in red and blue, respectively. Yellow dots indicate ECM proteins. (F) Heatmap of differentially expressed ECM proteins. (G, H) Western blots of NID1 protein in Gli1-Smo+/+ and Gli1-Smo-/- or in Pdgfrβ-Smo+/+ and Pdgfrβ-Smo-/- kidneys at 1 day after IRI. Numbers indicate individual animals in a given group. (I) Single nucleus RNA sequencing showing NID1 mainly expressed by fibroblasts (Fib) and pericytes (Per) at 12 hours after IRI. (Data were extracted from the online database provided by Dr. Benjamin Humphrey's laboratory, http://humphreyslab.com/SingleCell/displaycharts.php) (J) Immunohistochemical staining showing NID1 protein expression in Gli1-Smo+/+ and Gli1-Smo-/- or in Pdgfrβ-Smo+/+ and Pdgfrβ-Smo-/- kidneys at 1 day after IRI. Arrows indicate positive staining. Scale bar, 25 µm. (K) Immunoprecipitation revealing that Smo binds to NID-1. NRK-49F cells under CoCl2 stress were immunoprecipitated with Smo or NID-1 antibody, followed by immunoblotting with antibody against NID-1 (left blot) or Smo (right blot). Differences among groups were analyzed using unpaired t-tests.
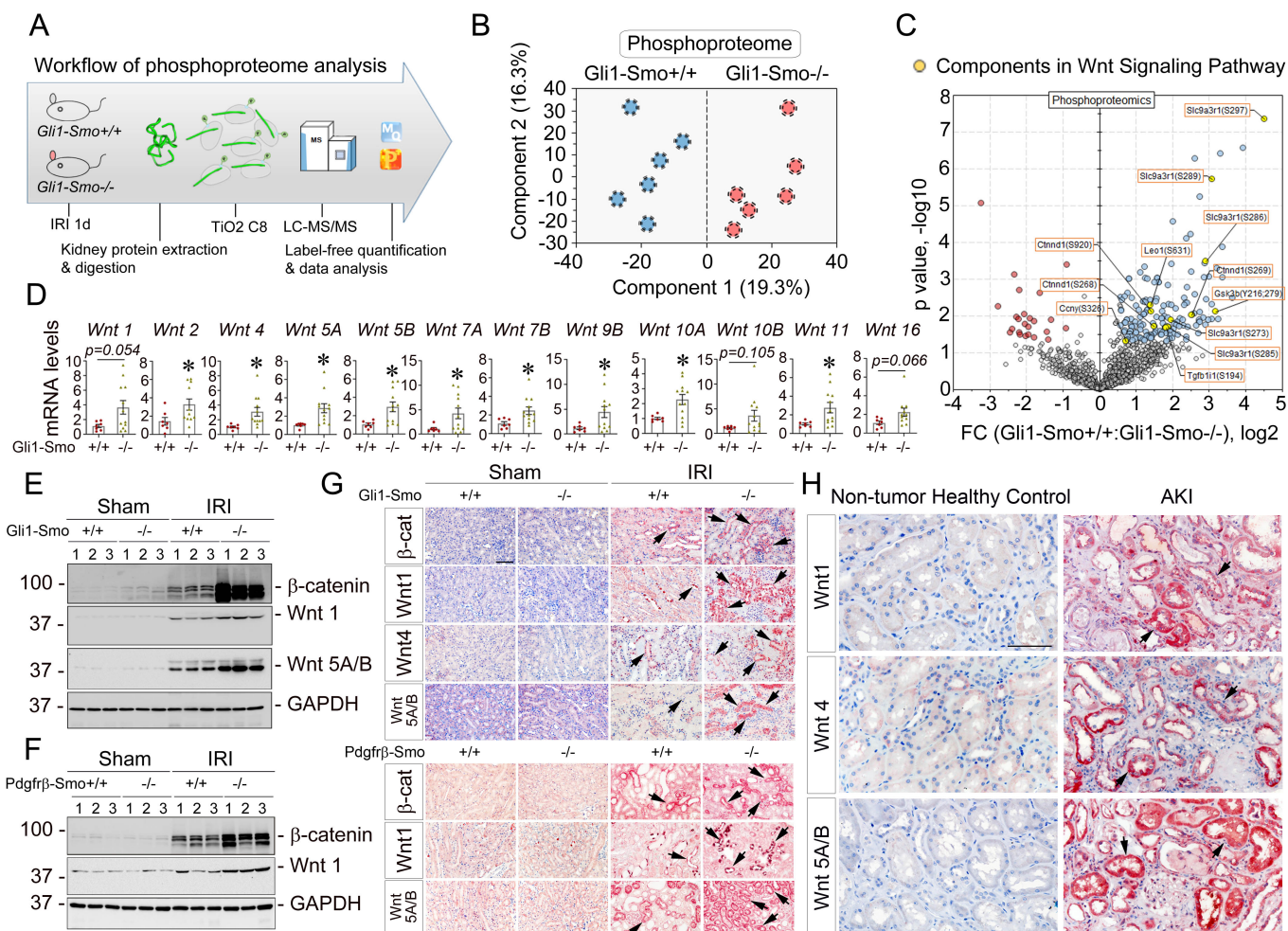
Figure 4: Phosphoproteomics reveals Wnt pathway activation in fibroblast-specific Smo deletion kidneys after AKI. (A) Workflow of phosphoproteomics. (B) Principal component analysis of phosphoproteins from Gli1-Smo+/+ and Gli1-Smo-/- kidneys at 1 day after ischemic AKI. (C) Volcano plot of pairwise comparisons (FC, fold-change) between the kidney phosphoproteomes of Gli1-Smo+/+ and Gli1-Smo-/-kidneys at 1 day after ischemic AKI. (D) qPCR of Wnt 1, 2, 4, 5A, 5B, 7A, 7B, 9B, 10A, 10B, 11, and 16 mRNA in Gli1-Smo+/+ and Gli1-Smo-/- kidneys at 1 day after ischemic AKI. * P < 0.05 (n = 7-12). (E) Western blots of β-catenin, Wnt 1, and Wnt 5A/B proteins in Gli1-Smo+/+ and Gli1-Smo-/- kidneys at 1 day after ischemic AKI. Numbers indicate individual animals in a given group. (F) Western blots of β-catenin and Wnt 1 in Pdgfrβ-Smo+/+ and Pdgfrβ-Smo-/- kidneys at 1 day after ischemic AKI. Numbers indicate individual animals in a given group. (G) Immunohistochemical staining showing β-catenin, Wnt1, Wnt 4, and Wnt5A/B in Gli1-Smo+/+ and Gli1-Smo-/- or in Pdgfrβ-Smo+/+ and Pdgfrβ-Smo-/- kidneys at 1 day after ischemic AKI. (H) Immunohistochemical staining showing Wnt1, Wnt 4, and Wnt5A/B expression in kidney biopsy specimens from AKI patients. Arrows indicate positive staining. Scale bar, 25 µm. Graphs are presented as means ± SEM. Differences between groups were analyzed using unpaired t-tests.
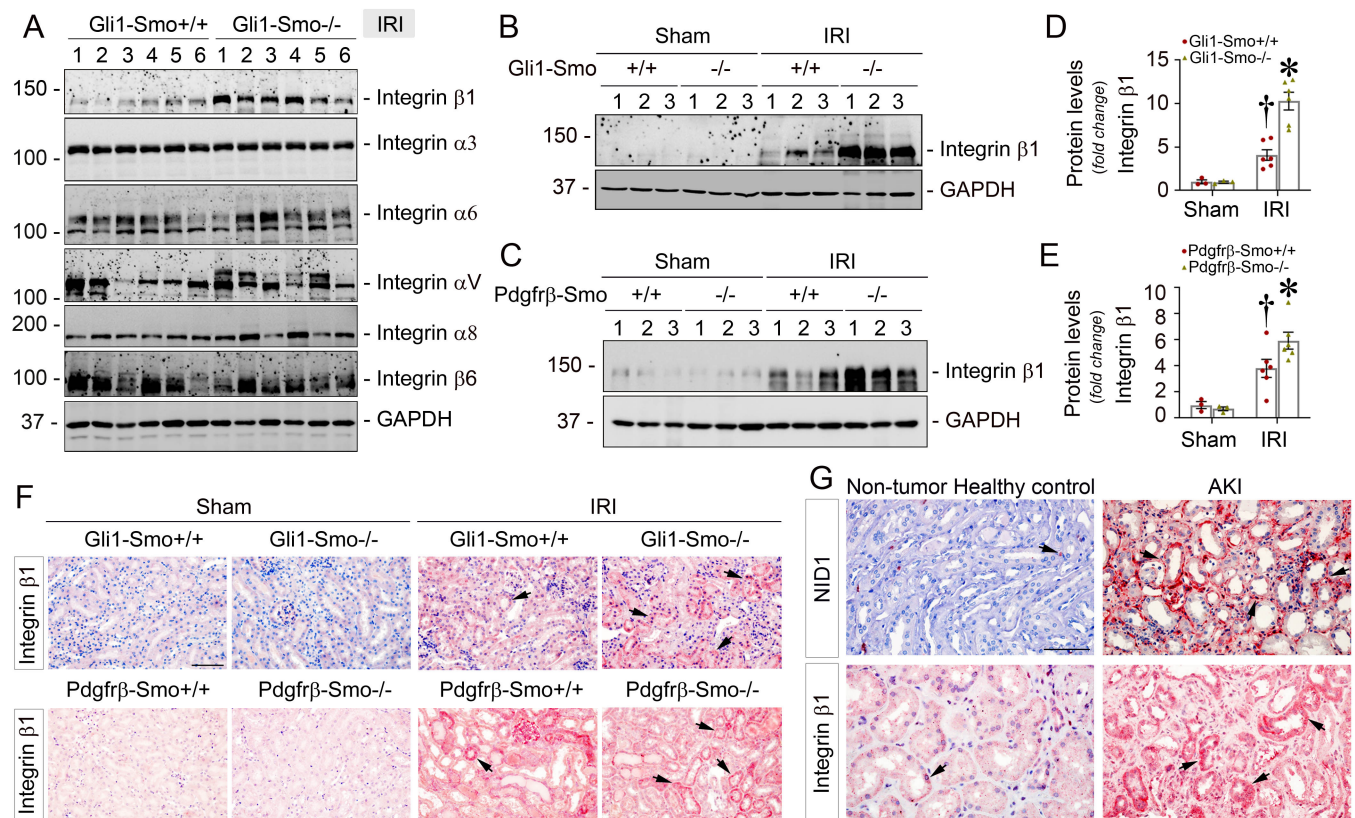
Figure 5: Deleting Smo in fibroblasts affects integrins linked to tubular cells after AKI. (A) Western blot assay showing the expression of integrin receptors linked to tubular cells, including integrin β1, α3, α6, αV, α8, and β6, in Gli1-Smo+/+ and Gli1-Smo-/- kidneys after ischemic AKI at 1 day. Numbers indicate individual animals in a given group. (B, C) Representative western blot showing the expression of integrin β1 in Gli1-Smo+/+ and Gli1-Smo-/- (B) or in Pdgfrβ-Smo+/+ and Pdgfrβ-Smo-/- (C) kidneys after 1 day after ischemic AKI. Numbers indicate individual animals in a given group. Quantitative data are accordingly presented in D and E. Dots indicate individual animals in a given group (Sham, n = 3; IRI, n = 6). † P < 0.05 versus sham control, * P < 0.05 versus Gli1-Smo+/+ or Pdgfrβ-Smo+/+ IRI mice. (F) Immunohistochemical staining showing integrin β1 in Gli1-Smo+/+ and Gli1-Smo-/- or in Pdgfrβ-Smo+/+ and Pdgfrβ-Smo-/- kidneys at 1 day after AKI. (G) Immunohistochemical staining showing NID1 and integrin β1 expression in kidney biopsy specimens from AKI patients. Arrows indicate positive staining. Scale bar, 25 μm. Graphs are presented as means ± SEM. Differences among groups were analyzed using one-way ANOVA, followed by the Student-Newman-Keuls test.
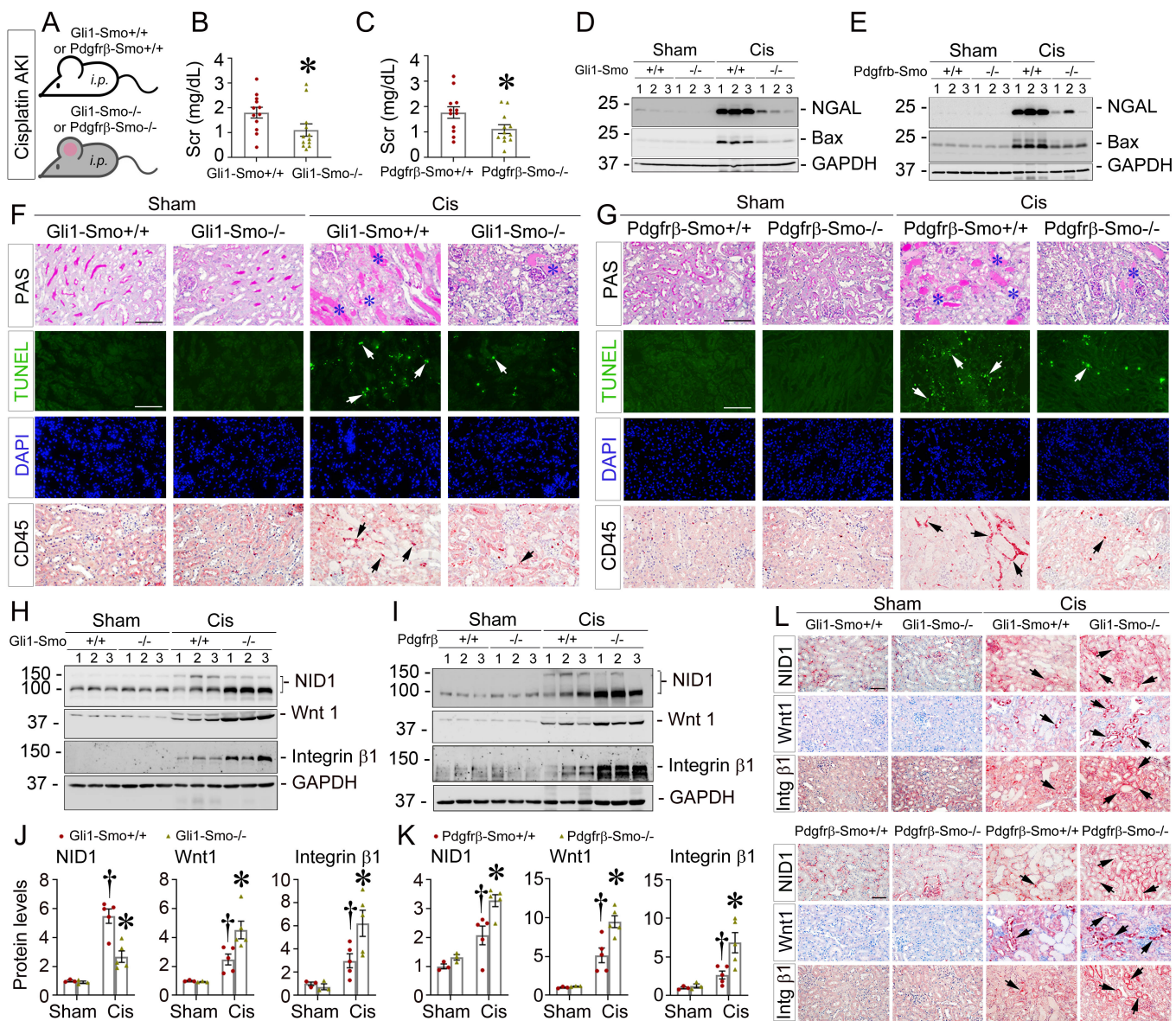
Figure 6: Specific deletion of Smo in fibroblasts mitigates AKI induced by cisplatin. (A) Schematic diagram. i.p., intraperitoneal. At 3 days after cisplatin (Cis) injection, (B) Serum creatinine (Scr) levels in Gli1-Smo+/+ and Gli1-Smo-/- mice (n = 12). (C) Scr levels in Pdgfrβ-Smo+/+ and Pdgfrβ-Smo-/- mice (n = 12). (D, E) Western blots assay showing NGAL and Bax protein levels in Gli1-Smo+/+ and Gli1-Smo-/- (D) or in Pdgfrβ-Smo+/+ and Pdgfrβ-Smo-/- (E) kidneys. (F) Periodic Acid–Schiff (PAS) staining showing kidney morphological changes in Gli1-Smo+/+ and Gli1-Smo-/- mice. Blue asterisks indicate injured tubules. Representative micrographs of TUNEL assay or immunohistochemical staining against CD45 in Gli1-Smo+/+ and Gli1-Smo-/- kidneys. (G) Representative micrographs of PAS staining, TUNEL assay, and immunohistochemical staining against CD45 in Pdgfrβ-Smo+/+ and Pdgfrβ-Smo-/- kidneys. (H, I) Western blots assay of NID1, Wnt1, and integrin β1 proteins in Gli1-Smo+/+ and Gli1-Smo-/- (H) or in Pdgfrβ-Smo+/+ and Pdgfrβ-Smo-/- (I) kidneys. Quantitative data are accordingly presented in J and K (Sham, n = 3; Cis, n = 5). † $P < 0.05$ versus sham control, * $P < 0.05$ versus Gli1-Smo+/+ or Pdgfrβ-Smo+/+ mice. Dots indicate individual animals in a given group. (L) Immunohistochemical staining showing NID1, Wnt1, and integrin β1 (Intg β1) in Gli1-Smo+/+ and Gli1-Smo-/- or in Pdgfrβ-Smo+/+ and Pdgfrβ-Smo-/- kidneys. Scale bar, 25 μm. Arrows indicate positive cells. DAPI is a nuclear counterstain. For all western blot panels, numbers indicate individual animals in a given group. Graphs are presented as means ± SEM. Differences among groups were analyzed using one-way ANOVA, followed by the Student-Newman-Keuls test.
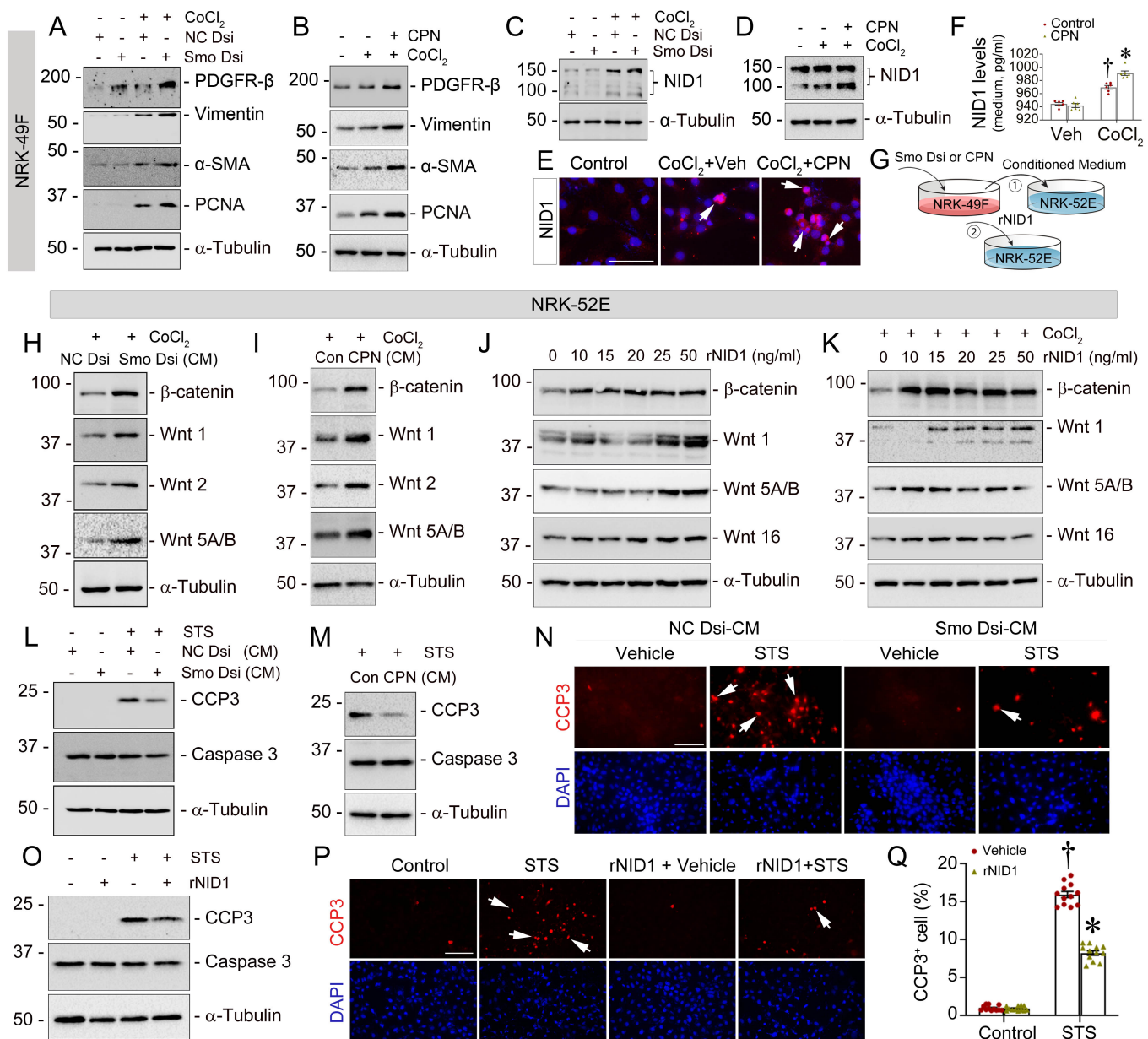
Figure 7: Nidogen-1 promotes Wnt components expression and reduces tubular cell death in vitro. (A-D) Normal rat kidney fibroblasts (NRK-49F) were transfected with Dicer-substrate Smo siRNA (Smo Dsi) or incubated with Smo inhibitor cyclopamine (CPN, 2.5 µM), then subjected to hypoxic stress (CoCl2, 400 µM) for 24 hours. Compared to control siRNA (NC Dsi) or vehicles, western blots demonstrating that knockdown (A) or inhibition (B) of Smo induced Pdgfrβ, vimentin, αSMA, and PCNA expression, and increased NID1 (C, D). (E) Immunofluorescence staining showing Smo inhibition induced NID1 in fibroblasts under hypoxic stress. (F) Enzyme-linked immunosorbent assay revealed NID1 concentration after incubation with CPN under hypoxic stress (n = 6). (G) Schematic diagram. (H, I) Western blots demonstrating β-catenin, Wnt1, Wnt2, and Wnt5A/B levels after knockdown (H) or inhibition (I) of Smo under hypoxic stress. (J, K) Western blots showing that NID1 recombinant protein (rNID1) elevated β-catenin, Wnt1, Wnt5A/B, and Wnt16 in cultured normal rat kidney proximal tubular cells at different dosages under basal conditions (J) and hypoxic stress (K). (L-M, O) After stimulation with staurosporine (1 µM) for 3 h, western blots assay showing reduced cleaved-caspase 3 (CCP3) in tubular cells incubated with NID1-enriched CM collected from Smo-knockdown (L) or CPN-treated (M) fibroblasts or directly treated with rNID1 (O). (N, P) Immunofluorescence staining showed fewer CCP3+ cells after treated with NID1-enriched CM (N) or NID1 recombinant protein (P). Quantitative data are presented in Q (n = 3, 4 random images were selected per slide, each dot represents the score of the according image). † $P < 0.05$ versus control, * $P < 0.05$ versus vehicle after STS. Scale bar, 25 µm. Cells were co-stained with DAPI. Arrows indicate positive staining. Graphs are presented as means ± SEM. Differences among groups were analyzed using one-way ANOVA, followed by the Student-Newman-Keuls test.
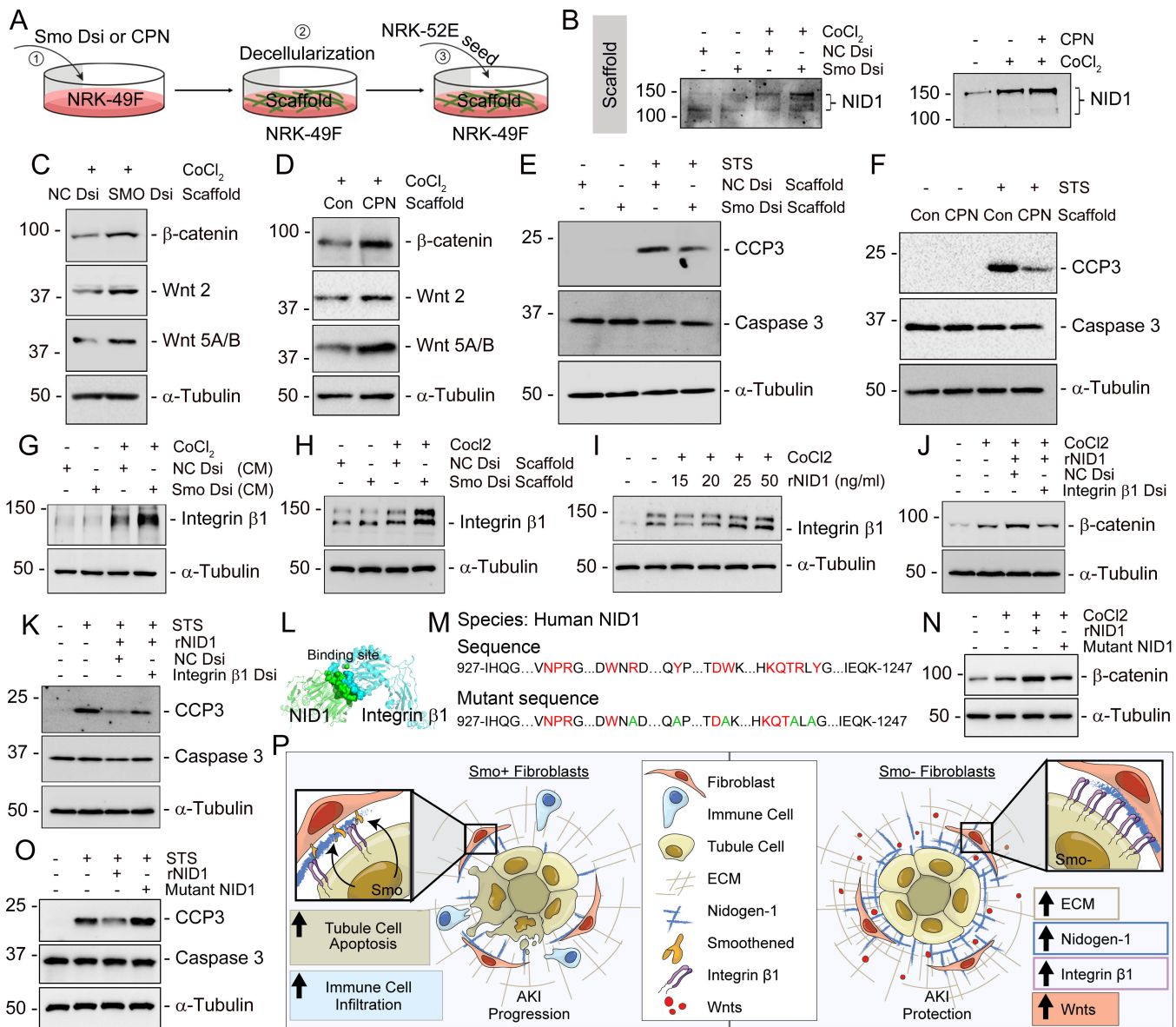
Figure 8: Nidogen-1-enriched decellularized fibroblast matrix scaffold activates Wnt components and reduces tubular cell death ex vivo. (A) Experimental design. ① normal rat kidney fibroblasts (NRK-49F) were transfected with Dicer-substrate Smo siRNA (Smo Dsi) or cultured with Smo inhibitor CPN to enrich for NID1; ② scaffolds were isolated; and ③normal rat kidney proximal tubular cells (NRK-52E) were seeded on top of scaffolds. (B) Western blots assay showing NID1 protein in decellularized fibroblast matrix scaffold. (C, D) Western blots assay showing β-catenin, Wnt2, and Wnt5A/B were activated in NRK-52E cells seeded on NID1-enriched matrix scaffold isolated from Smo-knockdown (C) or CPN-treated (D) fibroblasts under hypoxic stress. (E, F) Western blots assay showing NID1-enriched matrix scaffold isolated from Smo-knockdown (E) or CPN-treated (F) fibroblasts reduced cleaved caspase-3 (CCP3) in the seeded NRK-52E cells. (G-I) Western blots assay showing conditioned medium collected from Smo-knockdown fibroblasts (G) or decellularized fibroblast matrix scaffold isolated from Smo-knockdown fibroblasts (H) or NID1 recombinant protein (rNID1) increased integrin β1 in NRK-52E cells under hypoxic stress. (J, K) Under hypoxic stress, knockdown of integrin β1 using Dicer-substrate siRNA (integrin β1 Dsi) repressed β-catenin accumulation after incubation with rNID1 in NRK-52E cells (J) and induced CCP3 (K). (L) Molecular docking analysis showing the binding sites between NID1 and Integrin β1. (M) The strategy of designing a mutant form of NID1. (N, O) Compared to the active form of NID1 human recombinant protein (25 ng/ml), western blot assay demonstrating that mutant NID1 (25 ng/ml) failed to induce β-catenin expression in NRK-52E cells under hypoxic stress (N) and increased CCP3 after staurosporine (1 μM) stimulation (O). (P) Our model illustrates that loss of fibroblast-selective Smo promotes NID1 to interact with tubular integrin β1 and subsequently activated the Wnt signaling pathway in tubules by which forming a favorable microenvironment to protect against AKI.